 SID, vol.1, no.3, pp.225-231, 2005

Structural Integrity Analysis Using the Numerical Green's Function and the Local Boundary Integral Equation Method

L.S. Miers[1] and J.C.F. Telles[2]

Abstract: The present paper aims at introducing the concept of Green's function type fundamental solutions (i.e., unit source fundamental solutions satisfying particular boundary conditions) into the context of meshless approaches, particularly dealing with the local boundary integral equation method (LBIE) derived from the classic boundary integral equation procedure. The Green's functions discussed here are mainly the so-called half-plane solution, corresponding to a unit source within a semi-plane bounded by a flux-free straight line and an infinite plane containing internal lines of potential discontinuity. The latter is here introduced in numerical fashion, as an extension of the authors' previous numerical Green's function approach (NGF) already developed for standard fracture mechanics boundary element applications. Here, the use of such modified fundamental solutions impairs the implementation of the usual companion solutions, responsible for vanishing the fundamental potential values over the circular boundary of the LBIE internal support sub-domains. Some examples are discussed to validate the implementations.

keyword: Local boundary integral equation, numerical Green's function, meshless methods.

1 Introduction

Since the beginning of the utilization of numerical methods for solving differential equations, a common problem faced by researchers is mesh generation. However, instead of only developing more efficient mesh generation techniques, recently a number of researchers started working on meshless counterparts of previously established formulations [Atluri and Shen (2002); Atluri and Zhu (2000)]. One of these procedures is the so-called local boundary integral equation method – LBIE [Zhu, Zhang and Atluri (1998)], based on boundary integral equation formulations, from which also derives the boundary element method – BEM [Brebbia, Telles and Wrobel (1984)].

This paper aims at bringing the concept of the use of modified fundamental solutions (or Green's function – GF) to the LBIE context. These solutions can be used to simulate localized damages within the structure without need of element discretization of crack, or any other flaw, boundary. Two different kinds of GFs for potential problems are proposed, one is an exact solution for a unit source in a semi-infinite plane (or half-plane) [Telles and Brebbia (1981)] and the other is an approximated (numerical – NGF) solution for a unit source within an infinite plane with lines of potential discontinuity [Telles, Vera-Tudela and Guimarães (2002)]. These implementations represent a first step to a more general elastostatic fracture mechanics application. Some examples are included to illustrate the procedure.

2 Local boundary integral equation method

To demonstrate the formulation, only the linear Poisson equation is used, even though the approach is suitable for solving nonlinear problems as well. Poisson's equation can be written as

$$\nabla^2 u(\mathbf{x}) = p(\mathbf{x}), \mathbf{x} \in \Omega \tag{1}$$

and the boundary conditions

$$\begin{aligned} u &= \overline{u} \text{ on } \Gamma_u \\ \frac{\partial u}{\partial n} &= q = \overline{q} \text{ on } \Gamma_q \end{aligned} \tag{2}$$

Here, p is a domain distributed function, Ω the domain bounded by Γ and Γ_u and Γ_q the portions of the boundary with potential and flux prescribed respectively.

A weak formulation of the problem can be written as

$$\int_\Omega u^G \left(\nabla^2 u - p\right) d\Omega = 0 \tag{3}$$

[1] PEC-COPPE/UFRJ, Rio de Janeiro, RJ, Brazil – lsmiers@coc.ufrj.br

[2] PEC-COPPE/UFRJ, Rio de Janeiro, RJ, Brazil – telles@coc.ufrj.br

where u^G is the Green's function used as the test function for the weighted residual statement and u is the trial function. The test function satisfies the following equation

$$\nabla^2 u^G(\xi,\mathbf{x}) + \delta(\xi,\mathbf{x}) = 0 \tag{4}$$

in which $\delta(\xi,\mathbf{x})$ is the Dirac delta function.

By integrating eq.(3) by parts twice, the global boundary integral equation is obtained as follows

$$u(\xi) = \int_\Gamma u^G(\xi,\mathbf{x})\frac{\partial u(\mathbf{x})}{\partial n}d\Gamma - \int_\Gamma u(\mathbf{x})\frac{\partial u^G(\xi,\mathbf{x})}{\partial n}d\Gamma - \int_\Omega u^G(\xi,\mathbf{x})p(\mathbf{x})d\Omega \tag{5}$$

where n is the outward normal vector to Γ, $\mathbf{x} = [x, y, z]^T$ is the set of co-ordinates and $\xi = [x_\xi, y_\xi, z_\xi]^T$ is defined as the source point.

To obtain the local formulation of eq.(5), a local sub-domain Ω_s and its boundary $\partial\Omega_s$ are considered instead of Ω and Γ respectively, leading to the following form

$$u(\xi) = \int_{\partial\Omega_s} u^G(\xi,\mathbf{x})\frac{\partial u(\mathbf{x})}{\partial n}d\Gamma - \int_{\partial\Omega_s} u(\mathbf{x})\frac{\partial u^G(\xi,\mathbf{x})}{\partial n}d\Gamma - \int_{\Omega_s} u^G(\xi,\mathbf{x})p(\mathbf{x})d\Omega \tag{6}$$

Eq.(6) indicates that the value of the unknown function at ξ can be obtained by carrying out the integrals over a sub-domain within the closed boundary Γ.

It should be noted that eq.(6) holds regardless of the shape and size of $\partial\Omega_s$, which can be deliberately chosen according to the characteristics of the functions used in the method. The most regular shape of a sub-domain is an n-dimensional sphere, centered at ξ, for a problem defined on an n-dimensional space.

For 2-D potential problems, Ω_s is a circle of radius r_0, and the Green's function and its normal derivative are

$$u^G = -\frac{1}{2\pi}\ln(r) + u^C$$
$$\frac{\partial u^G}{\partial n} = -\frac{1}{2\pi r}\frac{\partial r}{\partial n} + q^C \tag{7}$$

where u_c an q_c are the complementary solutions for potential and flux respectively, which are added to the classic fundamental solutions in order to obtain the Green's function corresponding to the desired problem. The use of the Green's function instead of the conventional fundamental solution precludes the use of the so-called "companion" solution [Atluri and Zhu (2000); Zhu, Zhang and Atluri (1998)], which is commonly added to the fundamental solution in order to make it vanish over the circular part of the sub-domain boundary $\partial\Omega_s$.

When ξ lies on the global boundary Γ, the sub-domain can still be taken as a part of a circle centered at ξ, but now its boundary includes the part of the circumference (L_s) and the part of Γ limiting $\Omega_s(\Gamma_s)$. The local integral equation for a nodal point ξ at Γ becomes

$$\alpha(\xi)u(\xi) = \int_{\Gamma_s+L_s} u^G(\xi,\mathbf{x})\frac{\partial u(\mathbf{x})}{\partial n}d\Gamma - \int_{\Gamma_s+L_s} u(\mathbf{x})\frac{\partial u^G(\xi,\mathbf{x})}{\partial n}d\Gamma - \int_{\Omega_s} u^G(\xi,\mathbf{x})p(\mathbf{x})d\Omega \tag{8}$$

where $\alpha(\xi)$ is a free coefficient depending on the shape of Γ at ξ.

3 Moving least squares approximation scheme

The method used to approximate the trial function is the so-called moving least squares (MLS) scheme [Atluri and Shen (2002); Atluri and Zhu (2000); Zhu, Zhang and Atluri (1998)]. A brief summary is given in what follows.

Consider a sub-domain Ω_x, in the neighborhood of a point ξ (called domain of definition of ξ), which is located entirely within Ω. The approximation of $u(\mathbf{x})$, namely $u^h(\mathbf{x})$, is taken over the nodes $\mathbf{x}_i$, i = 1,2, …, n, located within $\Omega_x$in the following form

$$u^h(\mathbf{x}) = \mathbf{p}^T(\mathbf{x})\cdot\mathbf{a}(\mathbf{x})\ \forall\mathbf{x}\in\Omega_x; \quad \mathbf{x}_i = [x_i, y_i, z_i]^T \tag{9}$$

where $\mathbf{p}^t(\mathbf{x})$ is a complete monomial basis of order m and $\mathbf{a}(\mathbf{x})$ is a vector of coefficients $a_j(\mathbf{x})$, j = 1, 2, …, m, which are function of the space coordinates. For 2-D problems,

$$\mathbf{p}^T(\mathbf{x}) = \begin{cases} [1,x,y]\,; \text{ linear basis; } \mathrm{m}=3 \\ \left[1,x,y,xy,x^2,y^2\right]\,; \text{ quadratic basis; } \mathrm{m}=6 \end{cases} \tag{10}$$

The coefficient vector $\mathbf{a}(\mathbf{x})$ is determined by minimizing a weighted discrete L_2 norm, as follows

$$J(\mathrm{x}) = \sum_{i=1}^{n} w_i(\mathbf{x})\left[\mathbf{p}^T(\mathbf{x}_i)\cdot\mathbf{a}(\mathbf{x}) - \hat{u}_i\right]^2 = [\mathbf{P}\cdot\mathbf{a}(\mathbf{x}) - \hat{\mathbf{u}}]^T\cdot\mathbf{W}\cdot[\mathbf{P}\cdot\mathbf{a}(\mathbf{x}) - \hat{\mathbf{u}}] \tag{11}$$

where $w_i(\mathbf{x})$ is the weight function associated with node $\mathbf{x}_i$. Here, for simplicity, only the Gaussian distribution function is used as $w_i(\mathbf{x})$, it is defined as follows

$$w_i(\mathbf{x}) = \frac{e^{-\left(\frac{d_i}{c_i}\right)^{2k}} - e^{-\left(\frac{r_i}{c_i}\right)^{2k}}}{1 - e^{-\left(\frac{r_i}{c_i}\right)^{2k}}} \text{ for } 0 \le d_i \le r_i \quad \text{or}$$
$$w_i(\mathbf{x}) = 0 \quad \text{for } d_i \ge r_i \tag{12}$$

where $d_i = ||\mathbf{x} - \mathbf{x}_i||$, c_i is a constant that controls the shape of w_i, r_i is the size of the support of w_i associated with $\mathbf{x}_i$ and k is a parameter here chosen as 1. There are many other functions suitable for use in MLS approximation, like cubic and quadric spline functions [Atluri and Shen (2002); Atluri and Zhu (2000); Zhu, Zhang and Atluri (1998)], but for many applications found in the literature, the best results were obtained with the Gaussian function. Matrices $\mathbf{W}$ and $\mathbf{P}$ have the following structure

$$\mathbf{P} = \begin{bmatrix} \mathbf{p}^T(\mathbf{x}_1) \\ \mathbf{p}^T(\mathbf{x}_2) \\ \vdots \\ \mathbf{p}^T(\mathbf{x}_n) \end{bmatrix};$$
$$\mathbf{W} = \begin{bmatrix} w_1(\mathbf{x}) & 0 & \cdots & 0 \\ 0 & w_2(\mathbf{x}) & & \vdots \\ \vdots & & \ddots & 0 \\ 0 & \cdots & 0 & w_n(\mathbf{x}) \end{bmatrix} \tag{13}$$

and $\hat{\mathbf{u}}$ is a vector containing fictitious nodal values of $u^h(\mathbf{x})$

$$\hat{\mathbf{u}} = [\hat{u}_1, \hat{u}_2, \cdots, \hat{u}_n] \tag{14}$$

The stationarity of $J(\mathbf{x})$ in eq.(11) with respect to $\mathbf{a}(\mathbf{x})$ leads to

$$\mathbf{A}(\mathbf{x}) \cdot \mathbf{a}(\mathbf{x}) = \mathbf{B}(\mathbf{x}) \cdot \hat{\mathbf{u}} \tag{15}$$

where matrices $\mathbf{A}(\mathbf{x})$ and $\mathbf{B}(\mathbf{x})$ are defined as

$$\mathbf{A}(\mathbf{x}) = \mathbf{P}^T \cdot \mathbf{W}(\mathbf{x}) \cdot \mathbf{P} \;; \quad \mathbf{B}(\mathbf{x}) = \mathbf{P}^T \cdot \mathbf{W}(\mathbf{x}) \tag{16}$$

Rearranging eq.(15) and substituting in eq.(9),

$$u^h(\mathbf{x}) = \mathbf{p}^T(\mathbf{x}) \cdot \mathbf{A}^{-1}(\mathbf{x}) \cdot \mathbf{B}(\mathbf{x}) \cdot \hat{\mathbf{u}}$$
$$= \mathbf{\Phi}^T(\mathbf{x}) \cdot \hat{\mathbf{u}} = \sum_{j=1}^{n} \phi_j(\mathbf{x}) \hat{u}_j \tag{17}$$

where $\mathbf{\Phi}^T(\mathbf{x}) = \mathbf{p}^T(\mathbf{x}) \cdot \mathbf{A}^{-1}(\mathbf{x}) \cdot \mathbf{B}(\mathbf{x})$ is usually called shape function of the MLS scheme corresponding to the nodal source point.

4 Numerical implementation

Consider the parts of the global boundary Γ where the prescribed values are potential as Γ_u and flux as Γ_q. The intersections of these parts of Γ with the local subdomains Ω_s, for each source point (redefined as $\mathbf{x}_i$), are designated as Γ_{su} and Γ_{sq} respectively. Eq.(8) can then be rearranged, leading to the following system of equations

$$\alpha(\mathbf{x}_i)u(\mathbf{x}_i) = \int_{\Gamma_{su}} u^G(\mathbf{x}_i,\mathbf{x})\overline{q}(\mathbf{x})d\Gamma$$
$$- \int_{\Gamma_{sq}} \overline{u}(\mathbf{x}) \frac{\partial u^G(\mathbf{x}_i,\mathbf{x})}{\partial n} d\Gamma + \int_{\Gamma_{su}} u^G(\mathbf{x}_i,\mathbf{x}) \frac{\partial u(\mathbf{x})}{\partial n} d\Gamma$$
$$- \int_{\Gamma_{sq}} u(\mathbf{x}) \frac{\partial u^G(\mathbf{x}_i,\mathbf{x})}{\partial n} d\Gamma + \int_{L_s} u^G(\mathbf{x}_i,\mathbf{x}) \frac{\partial u(\mathbf{x})}{\partial n} d\Gamma$$
$$- \int_{L_s} u(\mathbf{x}) \frac{\partial u^G(\mathbf{x}_i,\mathbf{x})}{\partial n} d\Gamma - \int_{\Omega_s} u^G(\mathbf{x}_i,\mathbf{x}) p(\mathbf{x}) d\Omega \tag{18}$$

where $\overline{u}(\mathbf{x})$and $\overline{q}(\mathbf{x})$are the values of prescribed potential and flux. Substituting the trial function and its normal derivative by their MLS approximations, isolating the unknown terms on the left hand side, simplifying the notation and rearranging lead to the following system of equations

$$\mathbf{K}\hat{\mathbf{u}} = \mathbf{f} \longleftrightarrow \sum_{j=1}^{N} K_{ij}\hat{u}_j = f_i \quad (i = 1,2,\ldots,N) \tag{19}$$

where

$$f_i = \begin{cases} \int_{\Gamma_{su}} u_i^G \overline{q} d\Gamma - \int_{\Gamma_{sq}} \overline{u} \frac{\partial u_i^G}{\partial n} d\Gamma - \\ \int_{\Omega_s} u_i^G p d\Omega - \alpha_i \overline{u}_i \text{ where } u_i \text{ is known} \\ \int_{\Gamma_{su}} u_i^G \overline{q} d\Gamma - \int_{\Gamma_{sq}} \overline{u} \frac{\partial u_i^G}{\partial n} d\Gamma - \\ \int_{\Omega_s} u_i^G p d\Omega \text{ where } u_i \text{ is unknown} \end{cases} \tag{20}$$

and

$$K_{ij} = \begin{cases} \int_{\Gamma_{sq}} \phi_j \frac{\partial u_i^G}{\partial n} d\Gamma - \int_{\Gamma_{su}} u_i^G \frac{\partial \phi_j}{\partial n} d\Gamma - \\ \int_{L_s} u_i^G \frac{\partial \phi_j}{\partial n} d\Gamma + \\ \int_{L_s} \phi_j \frac{\partial u_i^G}{\partial n} d\Gamma \quad \text{where } u_i \text{ is known} \\ \\ \int_{\Gamma_{sq}} \phi_j \frac{\partial u_i^G}{\partial n} d\Gamma - \int_{\Gamma_{su}} u_i^G \frac{\partial \phi_j}{\partial n} d\Gamma - \\ \int_{L_s} u_i^G \frac{\partial \phi_j}{\partial n} d\Gamma + \int_{L_s} \phi_j \frac{\partial u_i^G}{\partial n} d\Gamma + \\ \alpha_i \phi_j(\mathbf{x}_i) \quad \text{where } u_i \text{ is unknown} \end{cases} \tag{21}$$

The system presented in eq.(19) can be solved by any conventional method, like Gauss elimination. Notice that the solution of the equations system is a vector $\hat{\mathbf{u}}$ containing the fictitious values $\hat{u}_i$ which must be post-processed using eq.(17) and its normal derivative in order to obtain the real values of potential and flux at all points.

5 Complementary solution

The complementary solution – $(\,)^C$ – is a function added to the fundamental solution– $(\,)^*$ – to generate the Green's function – $(\,)^G$ – suited to certain types of problems.

$$u^G(\xi,\mathbf{x}) = u^*(\xi,\mathbf{x}) + u^C(\xi,\mathbf{x})$$
$$\frac{\partial u^G(\xi,\mathbf{x})}{\partial n} = q^G(\xi,\mathbf{x}) = q^*(\xi,\mathbf{x}) + q^C(\xi,\mathbf{x}) \tag{22}$$

Here, two GFs for potential problems are proposed: an exact solution for a unit source in a semi-infinite plane and a numerical solution for an infinite plane containing unloaded lines of potential discontinuity.

5.1 Semi-infinite plane

In this work, the flux-free surface $\overline{\Gamma}$of the half-plane is assumed to be represented by a horizontal line. The complementary part for this problem is a function of the coordinates of the image of the load point with respect to$\overline{\Gamma}$ as shown in Fig.(1).

The complementary functions are shown as follows

$$u^C = -\frac{1}{2\pi}\ln(R)$$
$$\frac{\partial u^C}{\partial n} = q^C = -\frac{1}{2\pi r}\frac{\partial R}{\partial n} \tag{23}$$

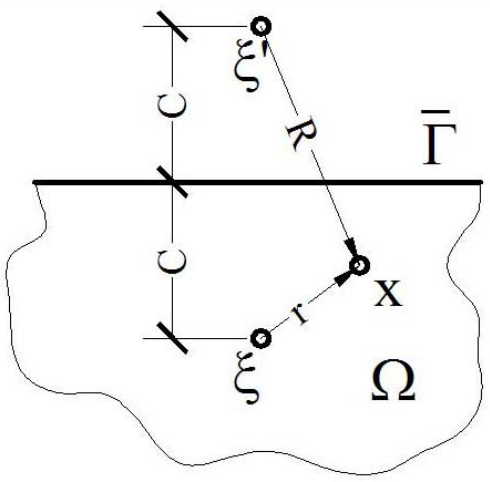

Figure 1 : half-plane GF

For more details, see [Telles and Brebbia (1981)].

5.2 Infinite plane with internal lines of potential discontinuity

Consider an infinite plane, with a line of potential discontinuity within, under the action of a unit point source applied at ξ. In what follows, the Green's function for this problem is written in terms of a superposition of the fundamental solution for Laplace's equation plus a complementary part which provides satisfaction of the flux-free requirement over the internal line of potential discontinuity (see Fig (2)).

The Laplace's solution u* and q* produces nonzero flux values across the barrier line $\Gamma^f(\zeta)$, these are then counterbalanced by the complementary fluxes. Hence, an infinite plane with an impervious slit is simulated.

The complementary part of the GF can be written in terms of boundary integral equations as

$$u^C(\xi,\mathbf{x}) = \int_{\Gamma^-} q^*(\mathbf{x},\zeta)\cdot c(\xi,\zeta)d\Gamma(\zeta)$$
$$q^C(\xi,\mathbf{x}) = \int_{\Gamma^-} Q^*(\mathbf{x},\zeta)\cdot c(\xi,\zeta)d\Gamma(\zeta) \tag{24}$$

where $q^*(x,\zeta)$ and $Q^*(x,\zeta)$ are the free (Laplace's) fundamental flux and its derivative referred to the source point as used in the classical and hypersingular boundary integral equations.

These equations produce the complementary potential and flux at an internal point **x** due to a unit point source

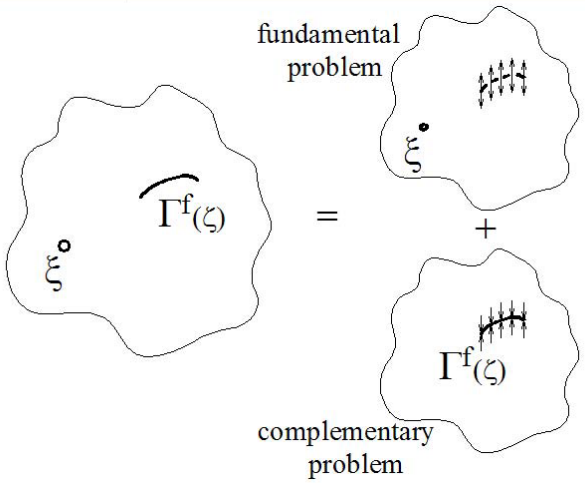

Figure 2 : NGF

at ξ, as a function of the potential discontinuity $c(\xi,\zeta) = u(\xi,\zeta^r) - u(\xi,\zeta^t)$. Note that here the source point of the complementary problem is **x**; point ξ is introduced only to guarantee that the complementary solution is computed with the same notation as eq.(22). The boundary Γ^- corresponds to the inferior surface of the line of potential discontinuity, whose superior surface is Γ^+. The numerical value of $c(\xi,\zeta)$ is computed using an efficient implementation of the hypersingular boundary integral equation.

Complete details of the procedure can be found in [Telles, Vera-Tudela and Guimarães (2002)].

6 Examples

To illustrate the presented techniques, three examples are proposed using the two Green's functions. The results are compared with sufficiently refined ones obtained with a BEM potential code using quadratic elements.

6.1 Plate with circular hole

This example is a symmetric perforated plate whose quarter-part is depicted in Fig.(3).

The comparison of results is presented in Fig.(4). The node cloud contains 57 points (30 along Γ and 27 within Ω) and the half-plane GF-LBIE, with $\overline{\Gamma}$coinciding with the top horizontal boundary, has been used.

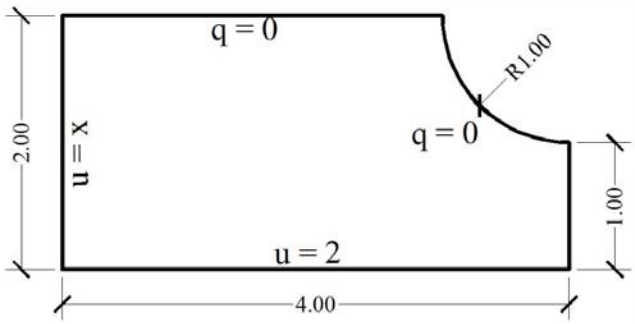

Figure 3 : quarter plate problem

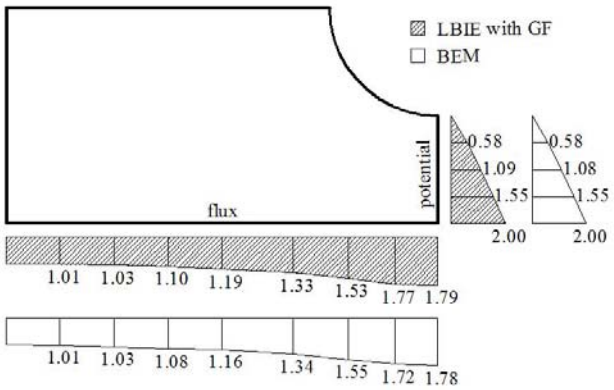

Figure 4 : quarter plate results

6.2 Plate with internal line of potential discontinuity

The geometry, node cloud and boundary conditions of this example are presented in Fig.(5).

The results obtained with NGF-LBIE and NGF-BEM techniques were very close and they are presented in Fig.(6).

6.3 Cofferdam-type problem

In this example there are two sheet piles enclosing a permeable soil to be excavated. The problem geometry is presented in Fig.(7). Because of the symmetry, only half of its geometry was analyzed. The node cloud and boundary conditions are presented in Fig.(8).

As in the last example, the results obtained with the NGF-LBIE and NGF-BEM were almost the same (see Fig.(9)).

7 Conclusions

As demonstrated by the results, the LBIE is shown to be suitable for a GF-procedure implementation. The de-

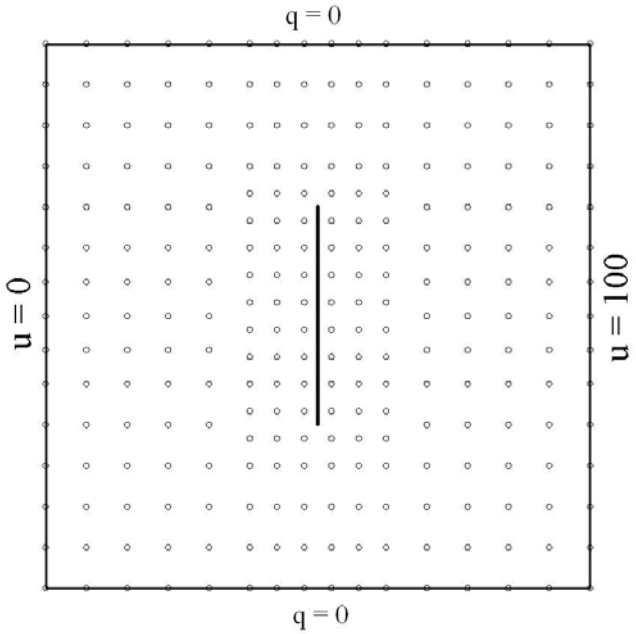

Figure 5 : plate problem

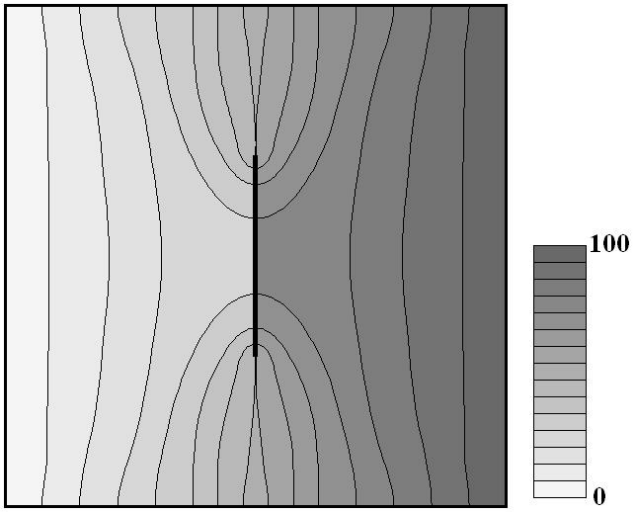

Figure 6 : plate problem potential results

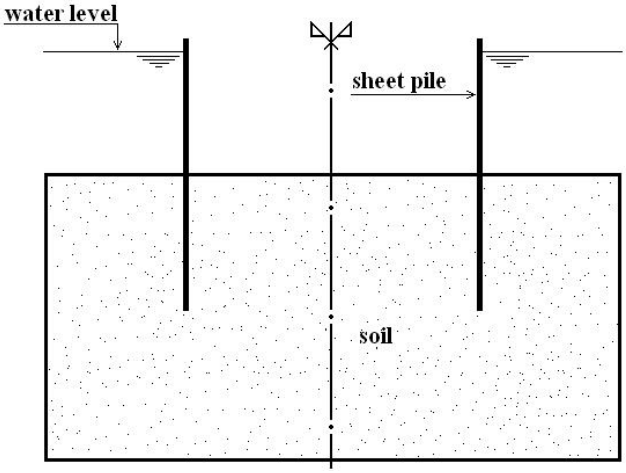

Figure 7 : cofferdam-type problem geometry

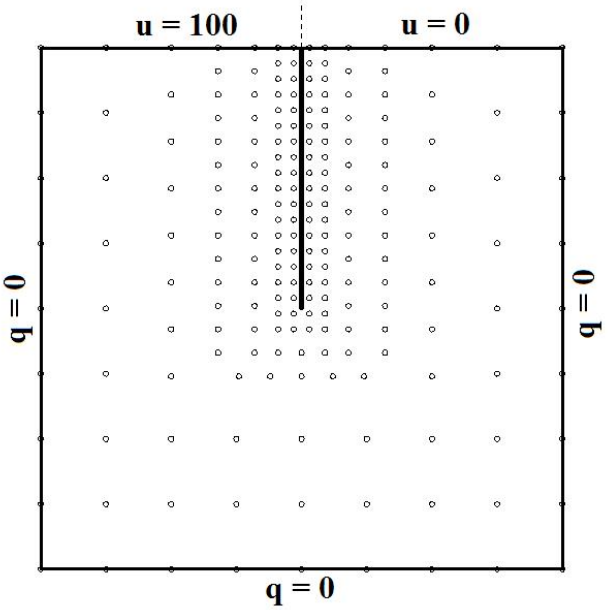

Figure 8 : cofferdam-type problem

velopment of the NGF for infinite planes with unloaded lines of discontinuity certainly has proved to be worth of attention, especially for elastic fracture mechanics applications.

References

Atluri, S.N.; Shen, S. (2002): The Meshless Local Petrov-Galerkin (MLPG) Method: A Simple & Less-costly Alternative to the Finite Element and Boudary Element Methods, *CMES: Computer Modeling in Engineering & Sciences*, vol. 3, pp. 11-51.

Atluri, S.N.; Zhu, T. (2000): New concepts in meshless methods, *Int. J. Num. Methods Engng.*, vol. 47, pp. 537-556.

Brebbia, C.A.; Telles, J.C.F.; Wrobel, L.C. (1984): Boundary Element Techniques: Theory and Applications in Engineering, Springer-Verlag, Berlin.

Telles, J.C.F.; Brebbia, C.A. (1981): Boundary element solution for half-plane problems, *Int. J. Solids Structs.*, vol. 17, pp. 1149-1158.

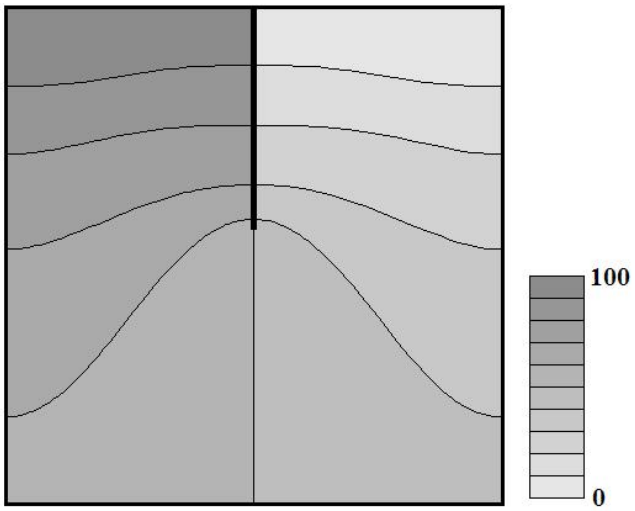

Figure 9 : cofferdam-type problem potential results

Telles, J.C.F.; Vera-Tudela, C.A.R.; Guimarães, S. (2002): Extended applications of the numerical Green's function BEM analysis, *Electronic Journal of Boundary Elements*, vol. BETEQ2001, No. 2, pp. 136-150.

Zhu, T.; Zhang, J.D.; Atluri, S.N. (1998): A local boundary integral equation (LBIE) method in computational mechanics, and a meshless discretization approach, *Computer Mechanics*, vol. 21, pp. 223-235.